Planar dual-band wide-scan phased array in X-band

Valavan, SE; Tran, DP; Yarovoy, A; Roederer, AG

DOI
10.1109/TAP.2014.2343252

Publication date
2014

Document Version
Accepted author manuscript

Published in
IEEE Transactions on Antennas and Propagation

Planar Dual-Band Wide-Scan Phased Array in X-Band

S. E. Valavan, D. Tran, A. G. Yarovoy, *Senior Member, IEEE* and A. G. Roederer, *Life Fellow, IEEE*

***Abstract*— The design of a planar dual-band wide-scan phased array is presented. The array uses novel dual-band comb-slot-loaded patch elements supporting two separate bands with a frequency ratio of 1.4:1. The antenna maintains consistent radiation patterns and incorporates a feeding configuration providing good bandwidths in both bands. The design has been experimentally validated with an X-band planar 9×9 array. The array supports wide-angle scanning up to a maximum of 60º and 50º at the low and high frequency bands respectively.**

***Index Terms*— Phased arrays, multi-frequency antennas, planar arrays, microstrip antennas.**

I. Introduction

RECONFIGURABLE multifunction radars are envisaged as the next generation of radar systems [1-5] and have attracted a large research interest in both industry and academia. The current trend is to enable several radar, and possibly, communication and positioning functions through the same aperture, which in turn requires the development of antenna arrays operating over two or more frequency bands. A number of ultra-wideband antenna arrays, similar to those in [6-9], have been proposed in literature responding to such needs. System demands however, would often be better satisfied (e.g. in terms of susceptibility to external electromagnetic interferences) by multi-band antenna arrays with well separated operational bands. The following performance goals are of particular interest for this research. Frequency ratios larger than or equal to 1.5:1 to exploit fully the X-band, with sub-band bandwidths greater than 250 MHz. Wide-angle scanning requirement of 50º, with a goal of 60º, along the principal planes, whereby, full azimuthal coverage is possible with four-faced array platforms. And finally, linearly-polarised antenna elements with cross polarisation levels of -15 dB or lower, along the principal operational planes. Since the primary focus is on surveillance radar applications, the design scope is limited to linearly-polarised antennas. The development and demonstration of dual- or multi-band antenna arrays have often been hindered by performance limitations of the antenna elements proposed. Many of the proposed dual- or multi-band array elements, some of the most common ones reviewed in [10-14], suffer from one of the four following performance limitations viz., very small frequency ratios between operational bands, large electrical dimensions at high frequency of operation, asymmetric or inconsistent radiation patterns in some or all bands and/or extremely narrow bandwidths at the operational bands [12, 14]. In this regard, the key objectives in this multilevel research can be hence summarised as follows: 1) design of array-capable antenna with suitable electrical dimensions and consistent radiation patterns, 2) verification of the antenna's scanning performance in infinite and finite arrays and 3) concept validation with array demonstrator.

In this paper, a novel concept of dual-band array element is proposed and validated experimentally with dual-band wide-angle-scanning array demonstrators. The validation is carried out at X-band, which is one of the bands of interest for several practical radar applications. Demonstrated performances include dual-band operation with a frequency ratio of 1.4:1, sub-band bandwidths greater than 250MHz, and wide-angle scanning up to 60º and 50º, along both the E- and H-planes, at the low and high frequency bands respectively. The dual-band comb-slot-loaded array element has optimal electrical dimensions to support wide-angle scanning, measuring only $0.38\lambda_L \times 0.38\lambda_L$ at the low frequency, with a simple and low-profile architecture. The combination of these features contributes to the novelty of the proposed array design.

II. Dual-Band Comb-Slot-Loaded Array Antenna

A. Antenna architecture

A concept to combine electric and magnetic radiator characteristics in a single antenna has been applied to the development of a dual-band patch antenna. To realize a magnetic radiator in a patch, a wide comb-shaped slot has been introduced. This enables the use of both the slot-based magnetic excitation and the patch-based electrical radiation characteristics in the overall radiation mechanism. The shape and sizes of both radiators (electric and magnetic ones) are selected to support two operational frequency bands. The radiating element, presented in Fig. 1a, consists of a metallic patch loaded with a four-arm comb-slot. The rationale behind the design of this slot shape can be explained as follows.

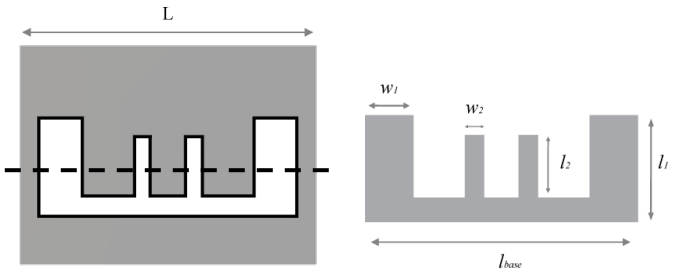

Fig. 1. (a)– Comb-slot-loaded patch and (b)– Four-arm comb-shaped patch.

Consider a metallic patch shaped similarly to the four-arm comb-slot, as shown in Fig. 1b. Exciting this patch by means of a simple pin-fed excitation over an infinite substrate and ground plane demonstrates the capability of this patch to support dual-resonances, as shown in Fig. 2. For the example

Manuscript received July 8, 2013, accepted July 18, 2014.

S. E. Valavan, D. Tran, A. G. Yarovoy and A. G. Roederer are with the Department of Electrical Engineering, Delft University of Technology, Mekelweg 4, 2628CD, Delft, Netherlands (e-mail: s.e.amaldoss@tudelft.nl).

This research is conducted as part of the Sensor Technology Applied in Reconfigurable systems for sustainable Security (STARS) project. For further information: *www.starsproject.nl.*

presented, the base length (l_{base} in Fig. 1b) was kept nearly equal to λ/2 at the 12 GHz (X-band).

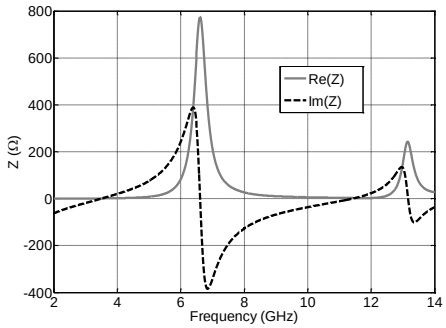

Fig. 2. Computed impedance response of comb-shaped patch antenna.

This comb-shaped patch radiator however, only supports electric radiation characteristics, similar to a typical patch antenna. To create an architecture supporting both electric and magnetic radiation characteristics, the complementary component of this comb-shaped patch, a comb-shaped slot, is loaded on to a metallic rectangular patch, as was shown in Fig. 1a. The design principle has previously been successfully applied for the development of CPW-fed ultra-wideband '*tulip-loop*' antennas [15]. Linear array implementations of this antenna have also been demonstrated [16].

There are two key aspects of the comb-slot-loaded patch design. First, the inner arms of the comb-slot help achieve band notch characteristics, which result in dual-band operation with low-profile electrical dimensions. The absence of these arms would result in a u-slot arrangement, as in [11]. The widths (w_1 and w_2) can be varied to tune the frequency ratio between the bands, whereas the lengths (l_1 and l_2) can be used to vary the impedance matching achieved in the operational bands. Furthermore, this comb-slot-loaded element makes it possible to support slot-based magnetic radiation, along with the patch-based electric radiation in both operational bands. While the combination of electric and magnetic radiators in a single element forms the first key aspect of the concept, a feeding architecture, providing simultaneous excitation of both electric and magnetic radiators, constitutes the other key aspect of the concept developed. The specifics of the radiation characteristics and feed configuration are described next.

B. *Feeding structure*

Exciting the comb-slot-loaded antenna with a pin feed, as used for other multi-band stand-alone antennas [10-14], would only result in an electric antenna, whereby, the slot's presence only aids in the modification of the surface current distribution in the operational bands. A modified L-probe feed with a capacitive matching ring arrangement is hence introduced into the antenna design. The components of the feed (Fig. 3a), designed to achieve both electric and magnetic radiation, include a plate-through-hole (PTH) cylinder, a field-matching ring and a stripline transition. The stripline transition, separated from the metallic patch by a dielectric layer, excites the comb-slot inducing the magnetic characteristics. This results in combined magnetic radiation from the comb-slot and electric radiation from the patch, with enhanced wide scan potential. As a consequence of the position of the stripline transition, the E- and H- planes of the antenna are defined along the *y-z* and *x-z* planes respectively (Fig. 3b). Finally, although the shape of the comb-slot has some resemblance with the u-slot designs, key functional differences exists in terms of the radiation characteristics and sub-band bandwidths, both of which will be demonstrated in the coming sections.

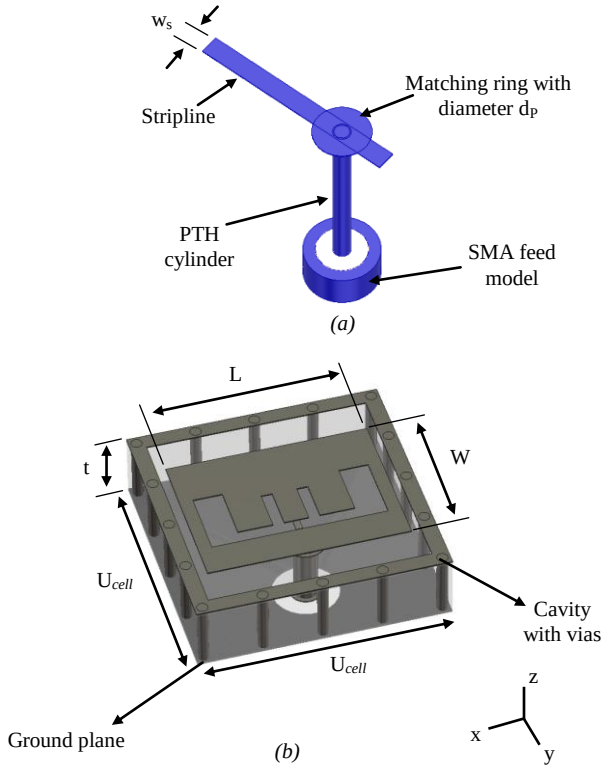

Fig. 3. Dual-band comb-slot-loaded antenna architecture. (a)- Feeding configuration and (b)- Unit-cell perspective view. Substrate maintained transparent for illustration.

Bandwidth enhancement

Another key feature of the proposed antenna is its inherent bandwidth enhancement capability in the operational sub-bands, achieved through the use of the feeding configuration. The plate-through-hole (PTH) cylinder results in an inductive reactance, similar to the pin-fed excitations in conventional patch antennas. The outer diameter of the PTH cylinder can be varied to tune the slope of the inductive reactance in the operational bands. The diameter of a standard SMA connector pin (1.28 mm) is used as the inner diameter of the PTH cylinder. This inductive reactance is balanced out by the capacitive reactance from the stripline. The matching ring diameter (d_p) presents an additional parameter for controlling the capacitive reactance, as required. Thus, this reactance balancing mechanism, made possible with the use of the components of the feeding apparatus, aids in achieving good bandwidths in the targeted operational bands. The optimization procedure to obtain the required sub-band bandwidths, involves the collective optimization of the width of the

stripline (w_s), matching ring diameter (d_p) and the height of the plate-through-hole (h_{PTH}) cylinder.

Other components of the antenna unit-cell (Fig. 3b) include the dielectric substrate, which is used in two parts, the first between the ground plane and the stripline transition, and a thinner substrate separating this transition from the metal patch above it. Cavity backing is added to the design for reducing mutual coupling in the array [17].

C. Stand-alone antenna performance

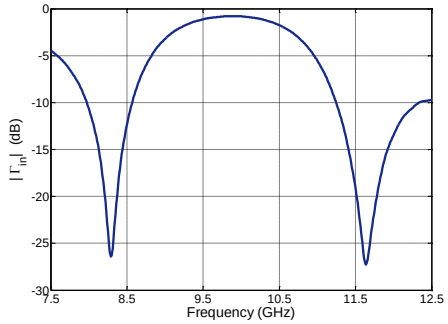

Fig. 4. Simulated input reflection coefficient ($|\Gamma_{in}|$) of the stand-alone dual-band antenna.

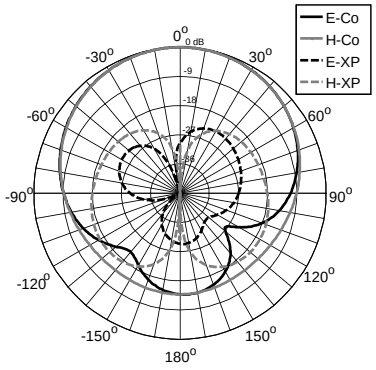

(a)

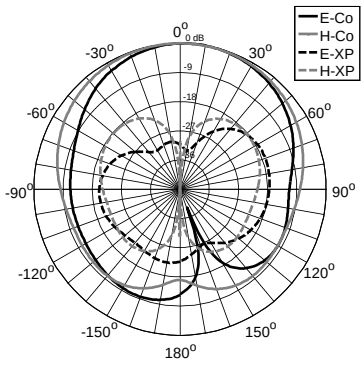

(b)

Fig. 5. Simulated radiation patterns of the stand-alone antenna element at (a)- 8.25 GHz and (b)- 11.5 GHz.

The computed performance summary of a stand-alone antenna (unit-cell), operational at X-band, is presented in Figs. 4 and 5. The antenna modelling was carried out in CST-MWS and a characteristic impedance of 50Ω was used for the simulations. A substrate with permittivity (ε_r) of 2.2 [18] was used for the antenna model. It can be inferred (from Figs. 4 and 5) that the antenna supports well-defined dual-band operation with consistent radiation patterns and a maximum frequency ratio of nearly 1.5:1. The inherent asymmetry of the comb-slot is largely responsible for the tilt in the radiation pattern along the E-plane at the high frequency band (Fig. 5b). The antenna hence achieves low-profile electrical dimensions, large frequency ratio and consistent embedded patterns suitable for wide-angle scanning, in line with the primary design objectives.

Slot-based radiation

To demonstrate the active role of the slot-based magnetic radiation in the overall radiation mechanism, the characteristics of the power flow distribution along the vertical z-axis (P_z) of the antenna's unit-cell is considered. The two-dimensional H-plane cut of the P_z component at the centre of the patch (the position of which is marked in Fig. 1a), at both the operational bands are presented in Fig. 6. It is clearly demonstrated that the net outward power flow, along the positive *z*-axis, exists inside the slot regions. The characteristic is existent in both the operational bands, the main difference being the comparatively stronger presence of the P_z component in the smaller inner arms in the low frequency band (Fig. 6a). The plots clearly demonstrate the role of the slot-based radiation in both the operational bands, illustrating the fundamental difference between the proposed comb-slot-loaded patch antenna and other dual- or multi-band patch antennas. Plane cuts at other locations outside the slot area exhibit a behavior similar to a usual patch-antenna and are hence not shown here for brevity.

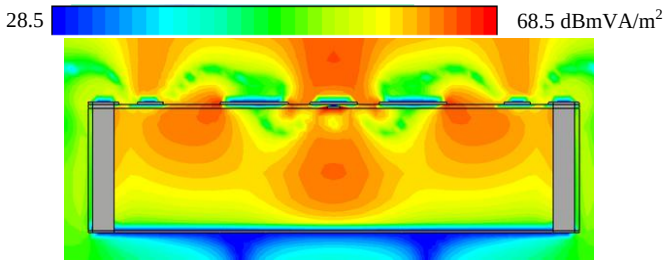

(a)

(b)

Fig. 6. Power flow distribution (P_z – component), H-plane cut. (a)– 8.25 GHz and (b)– 11.5 GHz.

The optimisation of the antenna was carried out in two steps, starting with the optimisation of the electrical dimensions of the antenna suitable for wide-angle scanning at both the bands. The length (L) of the patch is kept close to λ/2, in the high frequency band. The dimensions of the patch and of

the comb-slot arms are then optimised to achieve the necessary unit-cell dimensions. As previously mentioned, the widths of the comb-slot arms (w_1 and w_2) have strong influence on the frequency ratio between the bands, whereas, the lengths (l_1 and l_2) affect the impedance matching in the operational bands.

The second step involves the optimisation of impedance matching within the operational bands, which primarily depends on the concurrent optimisation of the width of the stripling (w_s), diameter of the matching ring (d_p) and the outer diameter and height (h_{PTH}) of the plate-through-hole cylinder (refer Fig. 3a). The impedance plot for the optimised stand-alone antenna is shown in Fig. 7. The impact of the reactance balance achieved through the use of the proposed feed device is evident from this plot. Low levels of reactance are achieved in the operational bands, which, in turn, facilitate in achieving the bandwidths (580 MHz and 990 MHz for stand-alone antenna) in the sub-bands.

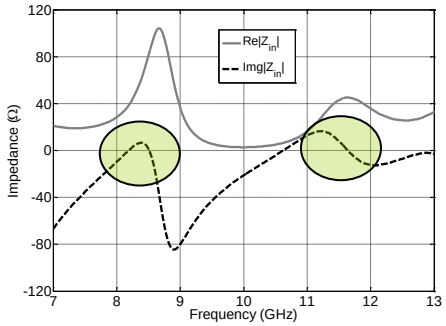

Fig. 7. Computed impedance (Z_{in}) plot of the dual-band array antenna.

D. *Infinite array performance*

Infinite array simulations were performed using CST-Microwave Studio (MWS) to optimise the scanning performance. The main design parameters (as mentioned in the previous section) were used for the optimisation. The variation of the active reflection coefficient ($|\Gamma_{act}|$) with scan angle is shown in Fig. 8. The performance is slightly more affected in the high frequency band along the E-plane, for a scan of 60º. We have already achieved a coupling level less than -20 dB in the high frequency band, along both planes of interest. To decrease the coupling level further the number of vias may be increased from five vias per side, as used in the model, to seven or nine vias per side; this however, would also complicate the fabrication process. The stronger 'in-air' coupling along the E-plane, compared to that along the D- and H-planes, and weaker field confinement within the unit-cell, due to the cavity via geometry, are both mainly responsible for the large perturbation of the reflection coefficient for a 60º scan (E-plane) at the high frequency band (Fig. 8). However, the dual-band performance is still maintained for this scan angle, albeit with a smaller bandwidth for the high band. It can hence be construed that beam scanning up to a maximum of 60º can be realistically expected from the array of this dual-band element.

Following this, finite array modelling was carried out with CST-MWS for the development of a prototype array demonstrator. A planar 9 × 9 array with rectangular grid was designed. The optimized antenna dimensions in millimetres are as follows: L = 12.5, W = 10.5, U_{cell} = 14.2 × 14.2, t = 4.2, d_p = 2.5, w_s = 0.45. The cavity lining width and via diameter are at 1mm and 0.7mm respectively. The substrate permittivity is ε_r = 2.2. This corresponds to unit-cell dimensions of the array element of 0.38λ × 0.38λ and 0.57λ × 0.57λ, at the lowest and highest frequencies of operation. The computed impedance matching performances for the 9 × 9 array are compared with measurements in the next section.

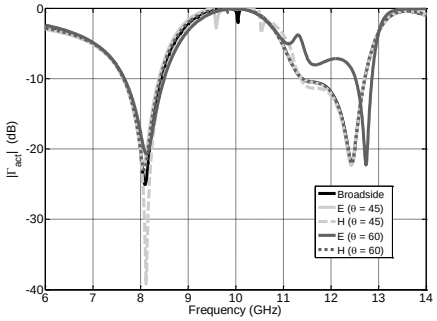

Fig. 8. Computed active input reflection coefficient ($|\Gamma_{act}|$) vs. scanning in the infinite array.

III. EXPERIMENTAL DEMONSTRATION

A. *Array prototype*

The fabricated 9 × 9 planar array prototype and its connector assembly are shown in Fig. 9. The array thickness is only 4.3mm, which translates into 0.117λ at the low frequency of operation. The planar array performance was measured in the anechoic chamber at TU-Delft, optimised for measurements in the 4–40 GHz range. A linearly polarised X-band horn antenna was used as the reference antenna for the pattern measurements.

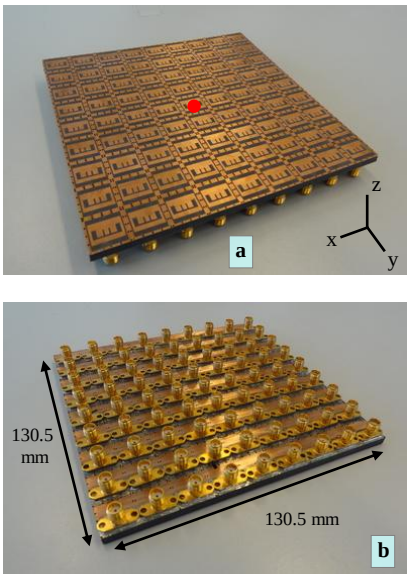

Fig. 9. Fabricated prototype demonstrator of the 9 × 9 dual-band planar array. (a) array face and (b) connector assembly.

B. *Measurement results*

The simulated and measured embedded reflection

coefficients of the array centre element (no: 41, marked with a red dot in Fig. 9a) are presented in Fig. 10. It can be seen that the antenna supports well-defined dual-band characteristics and also shows good agreement with the results of simulations. The measured bandwidths in the operational bands are 360 MHz and 650 MHz respectively, with a maximum frequency ratio of 1.4:1. The inclusion of the adhesive (bonding) layers in the numerical model plays a key role in ensuring conformance between the simulated and measured results. There is however, a difference in the frequency ratio, reduced from nearly 1.5:1 in the simulations to around 1.4:1 in the measurements. This can mainly be attributed to the slight differences in the substrate dielectric permittivity and components' dimensions due to fabrication tolerances. The active broadside reflection coefficient ($|\Gamma_{act}|$) of the centre element, calculated based on the measured embedded reflection coefficient and mutual coupling, is also presented in Fig. 10.

The embedded co- and cross-polarisation patterns along the E- (90°), H- (0°) and diagonal planes (45°) were measured in both the operational bands. A step increment of 1° was used for these measurements. The measured embedded patterns of the centre element (no: 41) at the centre frequencies of the sub-bands are presented in Figs. 11and 12 to demonstrate the consistency of radiation patterns. Measured cross-polarisation [19] levels below -17 dB are achieved in all the planes considered. The broad embedded patterns are well suited for wide-angle scanning, the performances of which are presented next. The measured patterns at other frequency points in the respective operational bands exhibit similar characteristics.

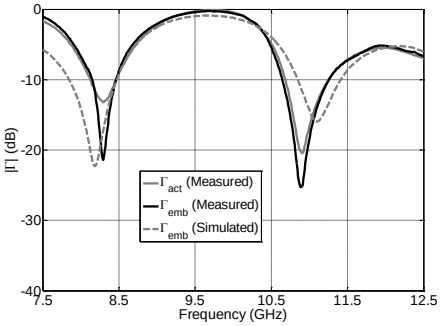

Fig. 10. Simulated and measured embedded reflection coefficient ($|\Gamma_{emb}|$) and broadside active reflection coefficient ($|\Gamma_{act}|$) of the centre element (no: 41) in the planar array.

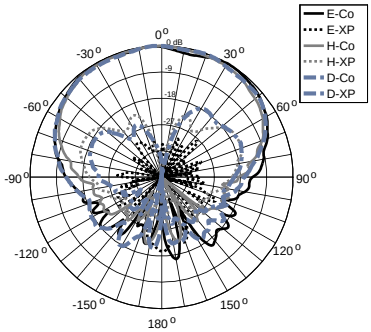

Fig. 11. Measured embedded pattern (centre element – no: 41) at 8.4 GHz (f_L).

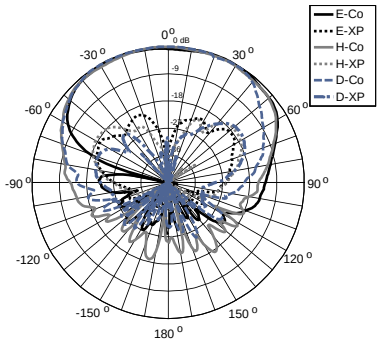

Fig. 12. Measured embedded pattern (centre element – no: 41) at 11 GHz (f_H).

The scanning performance of the array was evaluated using a post-processing Matlab script based on the measured embedded element patterns. Also, no tapering was applied for the calculations. The scanning performance of the array along the principal E-(*y*-*z*) and H-(*x*-*z*) planes at the centre frequencies of the sub-bands are presented in Figs. 13-16. It is demonstrated that the antenna supports wide-angle grating-lobe-free scanning up to a maximum of 60° and 50°, along both the E- and H-planes, in the low and high operational bands respectively. Similar scanning performances up to 60° and 50° are also achieved along the diagonal plane in the low and high frequency bands respectively. The sidelobe levels can be further controlled with the application of appropriate amplitude tapering, if required. The compact electrical dimensions of the dual-band array antenna and its broad embedded element patterns collectively aid in achieving this wide-scan performance. The measured cross-polarization levels are also attractive for surveillance radar applications, of particular interest for this research. The demonstrated wide-scan performance in both operational bands, even with a large frequency ratio (1.4:1), is a noteworthy feature of this dual-band phased array design.

IV. Conclusion

A dual-band phased array design supporting a frequency ratio up to 1.5:1 and scanning angles up to 60° has been proposed. A novel dual-band comb-slot-loaded antenna has been developed as an array element. It has low-profile architecture and electrical dimensions measuring 0.38λ × 0.38λ and 0.57λ × 0.57λ, at the lowest and highest frequencies of operation. The antenna exhibits consistent radiation patterns with low levels of cross-polarisation. A planar 9 × 9 array in X-band, developed to validate the performance, supports a frequency ratio of 1.4:1, and demonstrates wide-angle scanning up to a maximum of 60° and 50°, along both the principal E- and H-planes, at the low and high frequency bands respectively. Measured bandwidths of 360 MHz and 650 MHz are achieved for the low and high operational bands respectively. The large frequency ratio and wide-scan capability of the phased array make it suitable and attractive for future single-aperture multifunction radar front-ends. To the best of the authors' knowledge, the result presented, is one

of the first demonstrations of patch-based dual-band wide-scan phased arrays with a large frequency ratio.

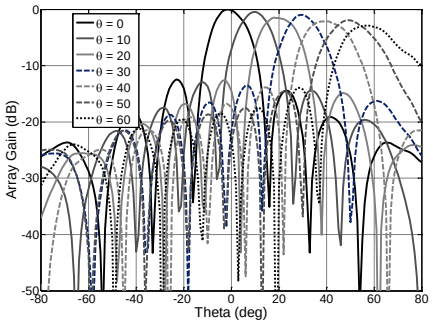

Fig. 13. Array (co-polarised) scanning performance based on measured embedded element patterns along E-plane (*y*-*z*) at 8.4 GHz (f_L).

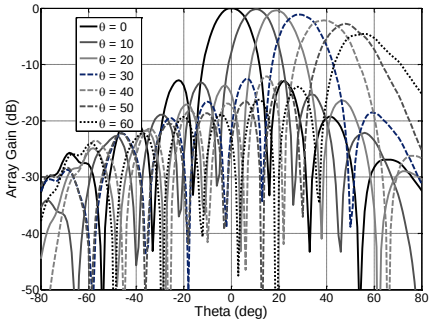

Fig. 14. Array (co-polarised) scanning performance based on measured embedded element patterns along H-plane (*x*-*z*) at 8.4 GHz (f_L).

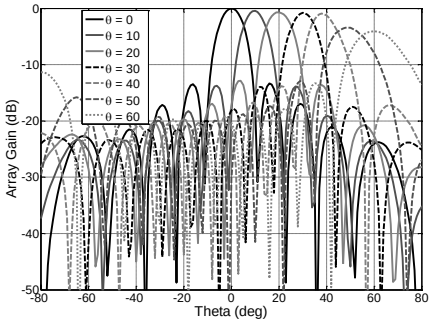

Fig. 15. Array (co-polarised) scanning performance based on measured embedded element patterns along E-plane (*y*-*z*) at 11 GHz (f_H).

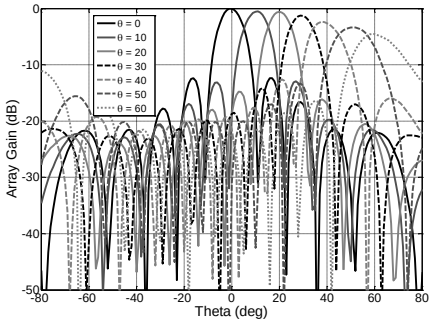

Fig. 16. Array (co-polarised) scanning performance based on measured embedded element patterns along H-plane (*x*-*z*) at 11 GHz (f_H).

V. Acknowledgement

The authors thank Pascal Aubry for his help with the demonstrator measurements and to the reviewers for their comments.

References

[1] J. Herd, D. Carlson, S. Duffy, M. Weber, G. Brigham, M. Rachlin, D. Cursio, C. Liss, C. Weigand, "Multifunction Phased Array Radar (MPAR) for aircraft and weather surveillance," *IEEE Radar Conference 2010*, vol., no., pp.945-948, 10-14, May 2010.

[2] A. Ouacha, A. Fredlund, J. Andersson, H. Hindsefelt, V. Rinaldi, C. Scattoni, "SE-IT joint M-AESA program: Overview and status," *Proc. of European Conference on Antennas and Propagation 2010*, vol., no., pp.1-5, 12-16, Apr 2010.

[3] A. Cetronio, M. D'Urso, A. Farina, C. Lanzieri, L. Timmoneri, M. Teglia, "Phased array systems and technologies in SELEX-Sistemi Integrati: State of art and new challenges," *IEEE International Symposium on Phased Array Systems and Technology (ARRAY)*, 2010, vol., no., pp.44-49, 12-15 Oct. 2010.

[4] S. Kemkemian, M. Nouvel-Fiani, "Toward common radar & EW multifunction active arrays," *IEEE International Symposium on Phased Array Systems and Technology (ARRAY)*, 2010 , vol., no., pp.777,784, 12-15 Oct. 2010.

[5] Raytheon Company. "Naval radars: Dual band radars (DBR)." Internet: http://www.raytheon.com/businesses/rids/businesses/scs/navalradars/dbr/index.html. 2012.

[6] B. Munk, R. Taylor, T. Durharn, W. Croswell, B. Pigon, R. Boozer, S. Brown, M. Jones, J. Pryor, S. Ortiz, J. Rawnick, K. Krebs, M. Vanstrum, G. Gothard, D. Wiebelt, "A low-profile broadband phased array antenna," *IEEE Antennas and Propagation Society International Symposium, 2003*, vol.2, no., pp.448-451, June 2003.

[7] S. S. Holland, D. H. Schaubert, Marinos N. Vouvakis, "A 7–21 GHz Dual-Polarized Planar Ultra-wideband Modular Antenna (PUMA) Array," IEEE Transactions on Antennas and Propagation, vol.60, no.10, pp.4589,4600, Oct. 2012.

[8] S. Livingston, J. J. Lee, "A wide band low profile dual-pol "Thumbtack" array," 2010 IEEE International Symposium on Phased Array Systems and Technology (ARRAY), vol., no., pp.477,483, 12-15 Oct. 2010.

[9] D. Cavallo, A. Neto, G. Gerini, "A 10.5–14.5 GHz wide-scanning connected array of dipoles with common-mode rejection loops to ensure polarization purity," *IEEE Antennas and Propagation Society International Symposium*, 2010, vol., no., pp.1-4, 11-17 July 2010.

[10] T. Chan, Y. Hwang, "A dual-band microstrip array antenna," *IEEE Antennas and Propagation Society International Symposium, 1995*, AP-S Digest, vol. 3, pp. 2132-2135, vol4, 1995.

[11] K. F. Lee, K. M. Luk, K. M. Mak, S. L. S. Yang, "On the use of u-slots in the designs of dual and triple-band patch antennas," *IEEE Antennas and Propagations Magazine*, vol.53, no.3, pp.60-74, June 2011.

[12] S. Maci, G.B. Gentili, "Dual-frequency patch antennas," *IEEE Antennas and Propagation Magazine*, vol.39, no.6, pp.13-20, Dec 1997.

[13] M. Veysi, M. Kamyab, A. Jafargholi, "Single-feed dual-band dual-linearly-polarized proximity-coupled patch antenna," *IEEE Antennas and Propagation Magazine*, vol.53, no.1, pp.90-96, Feb. 2011.

[14] K. Jhamb, L. Li, K. Rambabu, "Novel integrated patch antennas with multi-band characteristics," *IET Microwaves, Antennas and Propagation*, vol 5, no. 12, pp. 1393-1398, September 2011.

[15] D. Tran, F. Tanyer-Tigrek, A. Vorobyov, I. Lager and L. Ligthart, "A novel cpw-fed optimized UWB printed antenna," *European Conference on Wireless Technologies*, 2007, pp.40-43.

[16] F. Tanyer-Tigrek, I. Lager and L. Ligthart, "A cpw-fed printed loop antenna for ultra-wideband applications and its linear array performance," *IEEE Antennas and Propagations Magazine*, vol. 52, no. 4, pp.31-40, 2010.

[17] I.E. Lager, M. Simeoni, "Experimental investigation of the mutual coupling reduction by means of cavity enclosure of patch antennas," First European Conference on Antennas and Propagation, 2006. vol., no., pp.1,5, 6-10 Nov. 2006.

[18] Rogers Corporation. "Product selection guide." Internet: http://www.rogerscorp.com.

[19] A. Ludwig, "The definition of cross polarization," *IEEE Transactions on Antennas and Propagation*, vol.21, no.1, pp. 116- 119, Jan 1973.